Determination of Three-Dimensional Morphology and Inner Structure of Second-Phase Inclusions in Metals by Non-Aqueous Solution Electrolytic and Room Temperature Organic Methods

Jing Guo [1,2,*], Keming Fang [1], Hanjie Guo [1,2], Yiwa Luo [1,2], Shengchao Duan [1,2], Xiao Shi [1,2] and Wensheng Yang [1,2]

[1]   School of Metallurgical and Ecological Engineering, University of Science and Technology Beijing, Beijing 100083, China; fangkeming77@163.com (K.F.); guohanjie@ustb.edu.cn (H.G.); lyw918@126.com (Y.L.); metall_dsc@163.com (S.D.); mighty_works@163.com (X.S.); yws3179608@163.com (W.Y.)

[2]   Beijing Key Laboratory of Special Melting and Preparation of High-End Metal Materials, University of Science and Technology Beijing, Beijing 100083, China

[*]   Correspondence: guojing@ustb.edu.cn; Tel.: +86-10-62334964

Abstract: The secondary-phase particles in metals, particularly those composed of non-metallic materials, are often detrimental to the mechanical properties of metals; thus, it is crucial to control inclusion formation and growth. One of the challenges is determining the three-dimensional morphology and inner structures of such inclusions. In this study, a non-aqueous solution electrolytic method and a room-temperature organic technique were developed based on the principle of electrochemistry to determine the three-dimensional morphologies and inner structures of non-metallic inclusions in Al-killed steel, Si-killed steel, and ductile cast iron. The inclusions were first extracted without any damage to the inclusions, and then the collected inclusions were wrapped and cut through Cu ion deposition. The results revealed that the inclusions in Al-killed steel had an irregular morphology, that those in the Si-killed steel were mainly spherical, and that almost all the spheroidal graphite in the ductile cast iron featured a uniform globular morphology. In addition, nucleation was not observed in the inner structures of the inclusions in the Al-killed steel, while some dendritic or rod-like MnS phase precipitates appeared on the silicate inclusion surfaces, and some silicate-rich phases were detected in their inner matrix. For spheroidal graphite, rare-earth oxides (one particle or more) were observed as nuclei in the center of almost every graphite particle. The formation and evolution of inclusions in these types of metals can be better understood by means of the two developed methods.

Keywords: non-metallic inclusion; three-dimensional morphology; inner structures; non-aqueous solution electrolytic method; room temperature organic technique

1. Introduction

As secondary-phase particles, non-metallic inclusions are detrimental to the mechanical properties, fatigue life, and strip surface quality of steel. Many studies have explored inclusion morphology and inner structures with regard to non-metallic inclusion formation and growth mechanisms. Certain measures, such as limiting the precipitation or phase modification of the liquid phase, can be used to reduce the negative effects of such secondary particles, or even to render them beneficial to the overall steel product. The greatest challenge in this is that it is difficult to achieve an accurate three-dimensional morphology of the inclusions in the steel matrix. Metallographic methods are typically used to detect non-metallic inclusion properties in steels. By this method, one can only observe

the exposed two-dimensional face, which is used to approximate its three-dimensional properties, which include shape, size, and component distribution. Nevertheless, this method can access many different two-dimensional morphologies and sizes from different perspectives for the majority of known irregular inclusions.

Many researchers have attempted to develop additional techniques to detect more accurate morphologies and other information. Van Ende et al. [1,2] used HCl solution (1:1) to dissolve a steel matrix to extract its Al_2O_3 inclusions, and observed many interesting three-dimensional Al_2O_3 inclusion morphologies, thus deepening our understanding of Al_2O_3 inclusion nucleation and growth processes. Unfortunately, this method cannot be used to extract alkalescent oxide or sulfide inclusions, such as CaO-containing and CaS-rich ones, since they would be destroyed during the etching process. Fang et al. [3] developed a method using an organic electrolyte consisting of glycerine, triethanolamine, absolute methanol, and tetramethylammonium chloride solutions to extract inclusions in steel, confirming that the method could extract almost all the inclusions in a steel matrix without destruction of the inclusion morphology and chemical composition using an isotopic tracing method. Recently, Shi et al. [4] and Zhang et al. [5] applied this non-aqueous solution electrolytic method to separate the carbides from superalloy 718 and oxide-sulfide inclusions from linepipe steels.
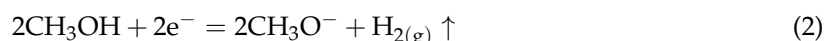
In addition to the three-dimensional morphology of the inclusions, the inner structure must also be understood to determine the inclusion formation and growth mechanisms. Although traditional two-dimensional metallographic methods can yield some information regarding inclusion inner structures, the methods have high contingency and very low efficiency. On the basis of non-aqueous solution electrolytic methods, the present authors developed a room temperature organic (RTO) technique to wrap and cut the collected inclusions on one plane in order to conveniently and effectively detect the inner structures of inclusions. Additionally, no matrix is measured around the inclusions except for Cu by means of the RTO technique. This could contribute to a more precise determination of inclusion composition than that achieved by classical metallographic methods.

In this study, the three-dimensional morphologies and inner structures of inclusions in Al-killed steels, Si-killed steels, and spheroidal graphite in cast iron were analyzed by applying both the non-aqueous solution electrolytic method and the RTO technique, and the morphology and inner structural characteristics are discussed based on the observed results.
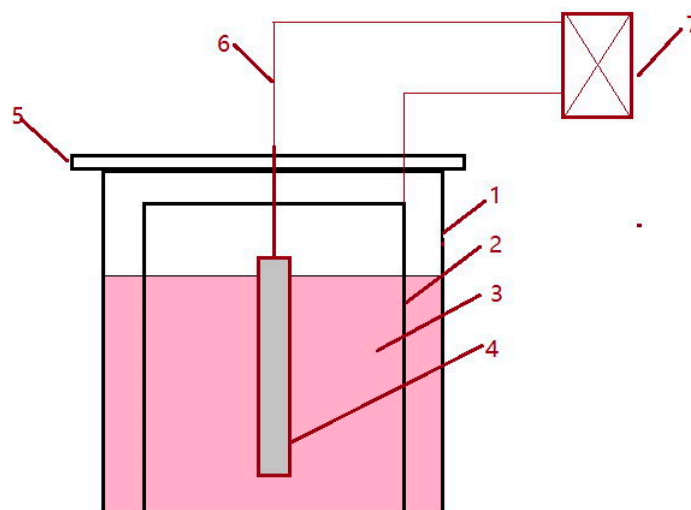
2. Experimental Methods

A non-aqueous solution electrolytic method was developed to extract the inclusions from the steel matrices to observe their three-dimensional morphology and surface characteristics. The apparatus for non-aqueous solution electrolysis is shown schematically in Figure 1.

Experimental alloy specimens were cut into cylinders 10 mm in diameter and 80 mm in length. The cylindrical alloy specimen was used as an anode, and a stainless-steel tube 50 mm in diameter and approximately 100 mm in length was used as a cathode. The cell reactions occurring on the anode and cathode are shown as Reactions (1) and (2), respectively.

$$Fe = Fe^{2+} + 2e^- \tag{1}$$

$$2CH_3OH + 2e^- = 2CH_3O^- + H_{2(g)} \uparrow \tag{2}$$

A type of anhydrous electrolyte solution was developed to avoid inclusion destruction during the electrolysis process, containing 4–10 vol % glycerine, 4–10 vol % triethanolamine, 80–92 vol % absolute methanol (anhydrous), and a small amount of tetramethylammonium chloride. During the experiment, the solution temperature was kept at 273–278 K (0–5 °C) and the electric current density on the steel surface was maintained below 200 mA/cm^2. A sufficient amount of inclusion particles could be extracted after 4 h of electrolysis. Thereafter, the inclusions in the remaining solutions were collected and prepared for scanning electron microscopy (SEM; EVO 18, ZEISS, Jena, Germany) or field emission scanning electron microscopy (FESEM; Supra 55, ZEISS, Jena, Germany) analysis.

Figure 1. Schematic of non-aqueous solution electrolysis for extraction of non-metallic inclusions in metals. 1—beaker, 2—stainless steel sheet, 3—solution, 4—specimen, 5—holder, 6—wire, 7—direct current power supply.
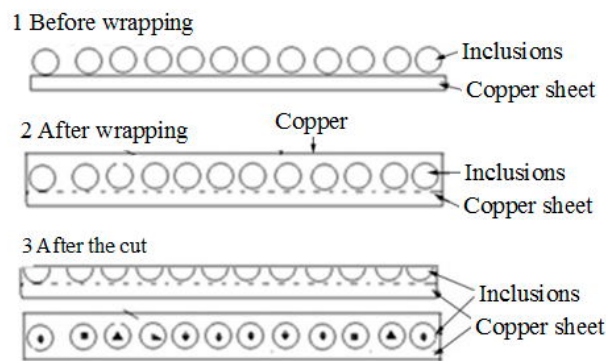
In order to determine the inclusion inner structure and characteristics, a RTO technique was used to wrap and cut the collected inclusions. First, the collected inclusions extracted by electrolysis were laid on a clean copper plate in a monolayer channeled by a vimineous glass tube 5 mm in diameter and 200 mm in length, which was then used as a cathode (another pure copper plate was used as an anode). The cell reactions on the anode and cathode in the RTO technique are shown as Reactions (3) and (4), respectively.

$$Cu = Cu^{2+} + 2e^- \tag{3}$$

$$Cu^{2+} + 2e^- = Cu \tag{4}$$

An electrolytic solution with similar composition as mentioned above was used at room temperature. An electric current lower than 500 mA was supplied using a direct current (DC) power source, and Cu was deposited on the collected inclusion layer-by-layer from the anode. Finally, the inclusions on the cathode copper plate were completely wrapped by Cu deposition. The cathode copper plate was then removed and ground using a very fine grit paper (more than 1000 grit number). As a result, the inclusions wrapped in the copper could be cut and their inner structures could be determined using SEM or FESEM. The main steps of the RTO technique are illustrated schematically in Figure 2, and the details of the two methods are summarized in Table 1.

Table 1. Summaries of non-aqueous (N-S) solution electrolytic and RTO methods.

Method	Functions	Anode	Cathode	Electrolyte Solution	Electric Current
N-S electrolytic	To extract inclusion	Specimen	Stainless steel tube	Organic solution	<200 mA/cm^2
RTO	To wrap and cut inclusion	Copper plate	Copper plate	Organic solution	<500 mA

Figure 2. Schematic of wrapping and cutting of the extracted inclusions by RTO technique.

In this work, the inclusions in Al-killed steel grades (A and B), Si-killed grades (C and D), and ductile cast iron (E) were investigated to better understand their present inclusions. Spheroidal graphite in cast iron was also considered a type of non-metallic inclusion in the present study, since they share common characteristics. The compositions of the five alloys are given in Table 2. All the alloy specimens were cut at the central part from a slab or an ingot, unless otherwise noted.

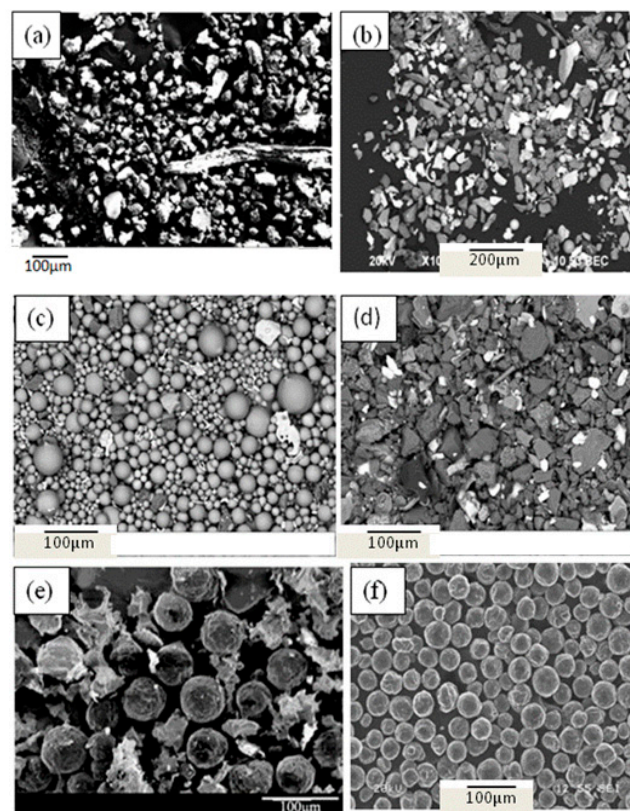**Table 2.** Compositions of alloys used in the present experiments (mass fraction %).

Steel Grade	C	Si	Mn	P	S	Al	Ti	Cr	Ni	Nb	RE
A	0.004	0.02	0.15	0.01	0.005	0.04	0.06	-	-	-	-
B	0.045	0.046	0.204	0.0097	0.006	0.041	-	-	-	-	-
C	0.10	0.35	1.48	0.017	0.007	-	-	-	-	0.01	-
D	0.05	0.50	1.10	0.011	0.003	-	-	18.22	8.10	-	-
E	4..20	1.07	0.20	0.005	0.003	-	-	-	-	-	9.32

3. Results and Discussions

Figure 3 shows the inclusion morphologies extracted from the five different alloys. The inclusions in Figure 3a were extracted from steel A. The main types of inclusions are Al_2O_3-based inclusions, TiN-based inclusions, and CaO-SiO_2-based inclusions, as identified by energy-dispersive X-ray spectroscopy. The inclusion diameters range from a few micrometers to more than 100 μm, and most of them have irregular morphologies. Figure 3b illustrates the inclusions extracted from steel B, in which a number of Al_2O_3-based and CaO-SiO_2-based inclusions with irregular morphology were detected. Some spherical SiO_2-MnO-CaO-Al_2O_3 multi-component inclusions were observed, as well, because of the Ca-treatment carried out in steel B. Figure 3c,d shows the inclusions in the continuously cast slab and hot-rolled sheet (3 mm in thickness), respectively, of steel C. Almost all the inclusions in the slab are spherical SiO_2-MnO-based inclusions, and the majority of them are deformed with irregular morphology after heat rolling. Figure 3e displays the inclusions extracted from steel D, which are mainly spherical in morphology and composed of CaO-SiO_2-MgO-Al_2O_3. Figure 3f presents the spheroidal graphite extracted from alloy E, which consists of nearly perfect spheroidals with homogenous morphology and size.

Figure 4 shows some typical individual inclusions extracted from the examined steels. The inclusions shown in Figure 4a–d were extracted from steel A, and are the most common inclusion types in steel A. Figure 4a shows a single Al_2O_3-based inclusion, which is faceted with an irregular morphology. Figure 4b presents a typical aggregated Al_2O_3-based cluster that consists of many small Al_2O_3 particles, while Figure 4c displays a TiN-based inclusion that is typically cubic and approximately 3 μm in size. Figure 4d depicts a typical CaO-SiO_2-based inclusion that also features small amounts of Na_2O and Al_2O_3. This type of inclusion usually has an irregular morphology and a relatively large size (>20 μm). Figure 4e shows three typical inclusion types in steel B: Al_2O_3-based, CaO-SiO_2-based, and SiO_2-MnO-CaO-Al_2O_3 multi-component inclusions, which are marked as 1,

2, and 3, respectively. Based on the inclusions observed in steel A and steel B, it is considered that more attention should be paid to limiting mold flux entrapment, since CaO-SiO$_2$-based inclusions are most likely to originate from mold flux entrapment. In addition, a number of irregular Al$_2$O$_3$-based inclusions would precipitate with a decrease in temperature during the solidification of Al-killed steels, even if Ca-treatment were carried out. Figure 4f,g depicts the typical inclusions extracted from steels C and D, respectively. Because steel C and steel D have similar chemical compositions, their inclusions are similar in composition (namely SiO$_2$-MnO-CaO-Al$_2$O$_3$) and have analogous spherical morphologies. The difference is that on the inclusion surfaces in steel C, many rod-like or granular MnS phase (white phase) precipitates surround the inclusion matrix, forming a net-like structure, as shown in Figure 4f, while almost no MnS precipitates can be observed on the inclusion surface of steel D, as shown in Figure 4g. In addition, very tiny dendritic structures can be detected in the inclusions in Figure 4g, suggesting that small crystals started to precipitate on the surface of the inclusion matrix during the solidification of steel D. Figure 4h,i presents the spheroidal graphite morphologies extracted from alloy E. Under high magnification, it can be seen that the graphite surface is not very smooth, and has many creases akin to blooming flowers, which are difficult to observe by traditional metallographic methods.
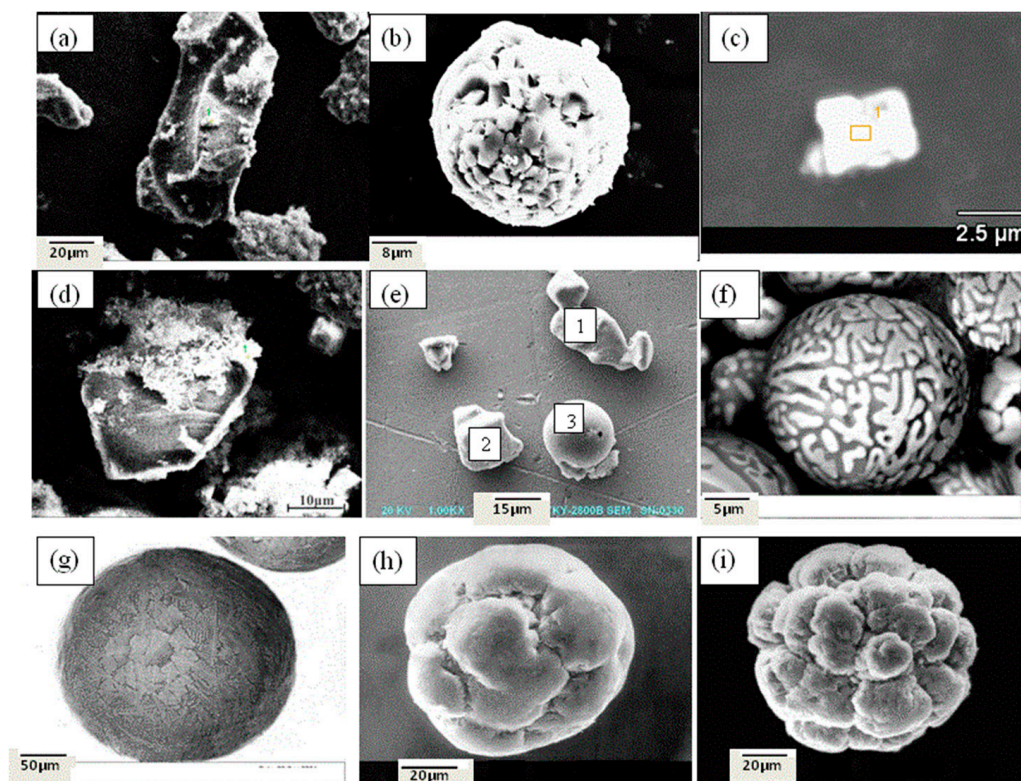

Figure 3. Morphologies of inclusions extracted from different steel grades, (**a**) steel A, (**b**) steel B, (**c**) steel C continuously cast slab, (**d**) steel C hot-rolled sheet, (**e**) steel D, and (**f**) steel E, using non-aqueous solution electrolysis.
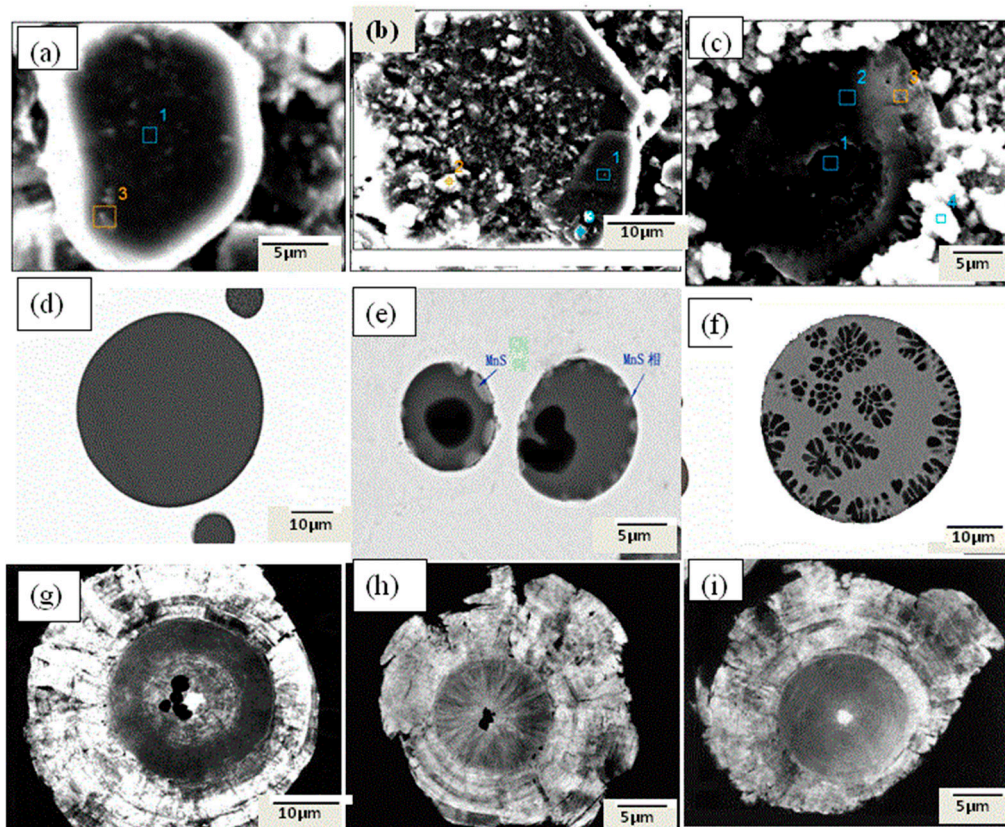
Figure 5 shows the inner morphologies of some typical extracted inclusions of the above alloys, after being cut using our RTO technique. Figure 5a,b shows the inner structures of individual and aggregated Al$_2$O$_3$-based inclusions, respectively. The individual Al$_2$O$_3$ inclusion is very dense, and no core was observed by SEM within the inclusion, while the aggregated sample was composed of many small Al$_2$O$_3$ particles with similar surface characteristics. Figure 5c presents the inner morphology of the CaO-SiO$_2$-based inclusion extracted from steel A, in which no inner secondary dendrite had precipitated within the inclusion, remaining as a glassy phase. Figure 5d–f shows some typical

inclusion inner structures extracted from steels C and D, respectively. These can be categorized into two typical types: all the components are either distributed homogeneously within the inclusion (Figure 5d), or else the spherical/spheroidal SiO_2-rich phases within the inclusion (dark phase) and a spindle-like MnS phase on the inclusion surface appear distinct from one another (Figure 5e). As shown in Figure 5f, the SiO_2-based phase precipitate formed many tiny dendritic structures both on the surface and within the second type of inclusion. By comparing the morphologies, it can be deduced that the inclusions in Figure 4f,g and those in Figure 5e,f are the corresponding inclusion types. These figures reveal that MnS precipitates on the SiO_2-MnO-based inclusion surface to form a dendritic structure as its three-dimensional morphology. Kim et al. [6] and Wang et al. [7] reported MnS-containing inclusions by metallographic methods that were very similar to that shown in Figure 5f; however, the three-dimensional morphology cannot be fully understood using only two-dimensional observations. In addition, SiO_2-rich phases precipitate as tiny dendritic structures both on the surface and as inner inclusions. Figure 5e,f confirms that the SiO_2-rich phases precipitate during solidification rather than as nucleis. In addition, Figure 5g–i shows the inner structure of spheroidal graphite. In the center of the spheroidal graphite, there are one or several rare-earth oxides acting as a crystal core, along with a dense graphite layer and an outermost relatively loose graphite layer. By employing these two methods, one can gain insight into the three-dimensional morphology and inner structures of inclusions, such as nucleus characteristics, thus deepening our understanding of spheroidal graphite formation and growth mechanisms in cast iron.

Figure 4. Three-dimensional morphologies of some typical individual inclusions extracted from different steel grades, (**a**) single Al_2O_3-based inclusion, (**b**) aggregated Al_2O_3-based cluster, (**c**) TiN-based inclusion, (**d**) CaO-SiO_2-based inclusion, (**e**) three typical inclusions in steel B, (**f**) rod-like or granular MnS phase precipitates surround the SiO_2-MnO-CaO-Al_2O_3 inclusion matrix, (**g**) tiny dendritic structures precipitating in the SiO_2-MnO-CaO-Al_2O_3 inclusion matrix surface, and (**h,i**) blooming flower-like spheroidal graphite.

Figure 5. Inner structures of some typical extracted inclusions cut by RTO technique, (**a**) single Al_2O_3-based inclusion, (**b**) aggregated Al_2O_3-based cluster, (**c**) CaO-SiO_2-based inclusion, (**d**) homogeneous spheroidal SiO_2-MnO-CaO-Al_2O_3 inclusion, (**e**) SiO_2-rich phases precipitating within the spheroidal SiO_2-MnO-CaO-Al_2O_3 inclusion and a spindle-like MnS phase on the inclusion surface, (**f**) tiny dendritic structure SiO_2-rich phases precipitating both on the SiO_2-MnO-CaO-Al_2O_3 inclusion surface and as inner inclusion, (**g–i**) one or several rare-earth oxides acting as a crystal core in the spheroidal graphites.

4. Conclusions

A non-aqueous solution electrolytic method and a RTO technique were developed in the present work and applied to investigating the three-dimensional morphology and inner structures of inclusions in Al-killed steel grades, Si-killed steel grades, and ductile cast iron. The following conclusions can be drawn from this study:

(1) The inclusions in Al-killed steel, Si-killed steel, and ductile cast iron can be extracted without destruction of their morphology and chemical composition, and their three-dimensional morphology and surface structure can be detected by SEM or FESEM. A RTO technique can be applied to cut the extracted inclusions and obtain more information regarding their inner structures.

(2) The majority of the inclusions in Al-killed steel slab had an irregular morphology, those in the Si-killed steel were mainly spherical, and almost all the spheroidal graphite in the ductile cast iron featured a uniform globular morphology.

(3) When the inclusions were cut by the RTO technique, nucleation was not observed in the inner structures of Al-killed steel. For silicate inclusions, some dendritic or rod-like MnS phase precipitates appeared on their surfaces, and some silicate-rich phases were detected in their inner matrix. For spheroidal graphite, rare-earth oxides (one particle or more) were observed in the center of almost every graphite particle as nuclei.

Author Contributions: Jing Guo, Keming Fang, and Hanjie Guo conceived and designed the experimental methods; Jing Guo, Yiwa Luo, Shengchao Duan, and Wensheng Yang carried out the experiments; Jing Guo and Keming Fang analyzed the experimental data; and Jing Guo wrote the paper.

Conflicts of Interest: The authors declare no conflict of interest.

References

1. Van Ende, M.-A.; Guo, M.X.; Proost, J.; Blanpain, B.; Wollants, P. Formation and morphology of Al_2O_3 inclusions at the onset of liquid Fe deoxidation by Al addition. *ISIJ Int.* **2011**, *51*, 27–34. [CrossRef]
2. Van Ende, M.-A.; Guo, M.X.; Zinngrebe, E.; Dekkers, R.; Proost, J.; Blanpain, B.; Wollants, P. Morphology and growth of alumina inclusions in Fe–Al alloys at low oxygen partial pressure. *Ironmak. Steelmak.* **2009**, *36*, 201–208. [CrossRef]
3. Fang, K.M.; Nan, R.M. Research on determination of the rare-earth content in metal phases of steel. *Metall. Mater. Trans. A* **1986**, *17*, 315–323.
4. Chen, X.C.; Shi, C.B.; Guo, H.J.; Wan, F.; Ren, H. Investigation of oxide inclusions and primary carbonitrides in Inconel 718 superalloy refined through electroslag remelting process. *Metall. Mater. Trans. B* **2012**, *43*, 1596–1607. [CrossRef]
5. Zhang, X.W.; Zhang, L.F.; Yang, W.; Wang, Y.; Liu, Y.; Dong, Y.C. Characterization of the Three-Dimensional Morphology and Formation Mechanism of Inclusions in Linepipe Steels. *Metall. Mater. Trans. B* **2017**, *48*, 701–712. [CrossRef]
6. Kim, H.S.; Lee, H.G.; Oh, K.-S. MnS precipitation in association with manganese silicate inclusions in Si/Mn deoxidized steel. *Metall. Mater. Trans. A* **2001**, *32*, 1519–1525. [CrossRef]
7. Wang, K.P.; Jiang, M.; Wang, X.H.; Wang, Y.; Zhao, H.Q.; Cao, Z.M. Formation Mechanism of SiO_2-Type Inclusions in Si-Mn-Killed Steel Wires Containing Limited Aluminum Content. *Metall. Mater. Trans. B* **2015**, *46*, 2198–2207. [CrossRef]